LANGMUIR

Article

pubs.acs.org/Langmuir

Fe_3O_4@PANI Hybrid Shell as a Multifunctional Support for Au Nanocatalysts with a Remarkably Improved Catalytic Performance

Chenjing Jin, Jie Han,* Fangyuan Chu, Xiaoxia Wang, and Rong Guo*

School of Chemistry and Chemical Engineering, Yangzhou University, Yangzhou, Jiangsu 225002, P. R. China

Supporting Information

ABSTRACT: Au@Fe_3O_4@PANI hybrid shells with controllable polyaniline (PANI) coatings as advanced supported catalysts have been fabricated. Specifically, Fe_3O_4 and Au nanoparticles were assembled on SiO_2 templates, followed by conducting polymer PANI coating, leading to the formation of Au@Fe_3O_4@PANI hybrid shells after the template removal. The resultant supported Au nanocatalysts not only maintain hollow structures but also possess high saturation magnetization (65.46 emu/g). Catalytic tests toward the reduction of 4-nitrophenol in the presence of $NaBH_4$ indicate that PANI and Fe_3O_4 not only endow high stability and recyclability but also can largely improve the catalytic activity of Au nanoparticles because of their synergetic effects. It is believed that Fe_3O_4@PANI hybrid shells can be regarded as multifunctional supports for noble metal nanocatalysts with a remarkably improved catalytic performance.

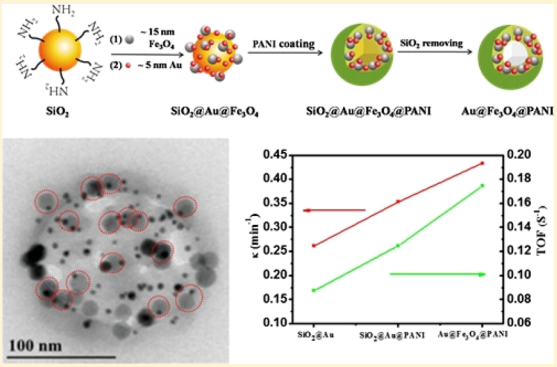

1. INTRODUCTION

Since the discovery of catalytic activity of Au nanoparticles toward CO oxidation,[1] noble metal nanoparticles have been extensively studied as nanocatalysts involved in numerous catalytic reactions.[2−5] As heterogeneous nanocatalysts, in addition to catalytic activity, recyclability and stability are also highly important from the economic and practical points of view. The most popular way is to introduce the typical superparamagnetic Fe_3O_4 microspheres as magnetic cores to improve the separation efficiency, followed by porous-structured materials coated with noble metal nanoparticles encapsulated in the channels or nanopores to avoid aggregation of neighboring nanocatalysts.[6−8] However, the improvement in recyclability and stability is always accompanied by the loss of catalytic activity of noble metal nanoparticles. Undoubtedly, the introduction of Fe_3O_4 microspheres can bring in magnetism; however, the nanochannels of porous shells will be blocked inside, which is adverse to diffusion and concentration of reagents involved in catalytic reactions and therefore resulting in decreased catalytic activity.[6] In addition, the synergistic effect toward improved catalytic activity of noble metal nanoparticles resulting from intact interfacial interaction between Fe_3O_4 and noble metal nanoparticles[9,10] has rarely been used.

Recently, Fe_3O_4−noble metal Janus nanostructures have aroused considerable attention because of their intriguing nanostructures and novel properties.[11,12] The interfacial interaction between Fe_3O_4 and noble metal nanoparticles has been established to contribute to the improved catalytic activity of noble metal nanoparticles. However, from the practical point of view as heterogeneous nanocatalysts, Fe_3O_4−noble metal Janus nanostructures still suffer from relatively low saturation magnetization. In addition, the dipole interactions between Fe_3O_4 nanoparticles will pull the adjacent Fe_3O_4 nanoparticles close to each other, resulting in aggregation. Although the construction of Fe_3O_4−noble metal Janus nanostructures can maintain the improved catalytic activity, the recyclability and stability remain unsolved.

Herein, we present a proof-of-concept demonstration that when Fe_3O_4 nanoparticles as the magnetic component are implanted in porous shells with compact interactions with noble metal nanoparticles, not only high saturation magnetization can be brought in but also the synergistic effect toward improved catalytic activity of noble metal nanoparticles can be exploited. Specifically, Fe_3O_4 and Au nanoparticles were assembled on SiO_2 templates, followed by conducting polymer polyaniline (PANI) coating, leading to the formation of Au@Fe_3O_4@PANI hybrid shells after the template removal. The choice of PANI as the porous shells is based on the facts that PANI can be synthesized in a facile and low-cost way with inherent porous structure because of its amorphous nature,[13−15] together with its conducting nature that can contribute to the improved catalytic activity of Au nanoparticles.[16] The magnetic component Fe_3O_4 with size down to 15 nm is chosen as it can form intact interactions with Au nanoparticles, which can also contribute to the improved catalytic activity of Au nanoparticles. Besides, numerous Fe_3O_4 nanoparticles assembled in a single Au@Fe_3O_4@PANI hybrid shell will guarantee high saturation magnetization. Catalytic

Received: February 24, 2017
Revised: March 30, 2017
Published: April 15, 2017

DOI: 10.1021/acs.langmuir.7b00640
Langmuir 2017, 33, 4520−4527

Scheme 1. Schematic Illustration of the Formation of Au@Fe_3O_4@PANI Hybrid Shells

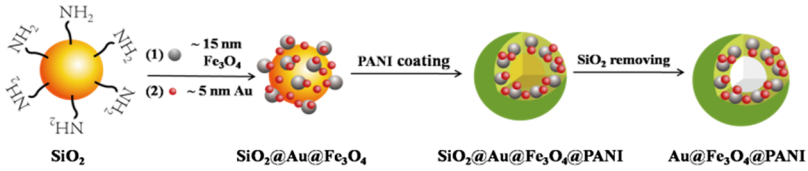

tests toward the reduction of 4-nitrophenol (4-NP) in the presence of $NaBH_4$ indicate that PANI and Fe_3O_4 not only endow high stability and recyclability but also can largely improve the catalytic activity of Au nanoparticles because of their synergetic effects. Results suggested that Fe_3O_4@PANI hybrid shells can be regarded as multifunctional supports for noble metal nanocatalysts with remarkably improved catalytic performance.

2. RESULTS AND DISCUSSION

2.1. Characterization of Au@Fe_3O_4@PANI Hybrid Shells. Scheme 1 outlines the general procedures for preparing Au@Fe_3O_4@PANI hybrid shells. First, the SiO_2 nanoparticles were synthesized using a modified Stöber method,[17] and the surfaces were modified with APTES. Monodisperse Fe_3O_4 (~15 nm) nanoparticles stabilized with oleic acid were prepared,[18] followed by replacing the oleic acid with DHCA.[19] Then, Fe_3O_4 nanoparticles can assemble on the surfaces of SiO_2 nanoparticles thanks to their electrostatic interactions. Au nanoparticles (~5 nm) were subsequently assembled on the surfaces of SiO_2@Fe_3O_4 nanoparticles, where most Fe_3O_4 nanoparticles were attached with Au nanoparticles. Aniline monomers were then added, followed by the chemical oxidation polymerization process after the addition of oxidants to yield PANI shells on the surface of SiO_2@Fe_3O_4@Au nanoparticles, leading to the formation of SiO_2@Au@Fe_3O_4@PANI core–shell hybrids. After the removal of SiO_2 templates, Au@Fe_3O_4@PANI hybrid shells can be fabricated.

The TEM images of the products obtained after each synthesis step were shown in Figure 1. Figure 1a displays the TEM image of the SiO_2 nanoparticles with a diameter of approximately 150 nm. Figure 1b,c shows the TEM images of the SiO_2@Fe_3O_4 and SiO_2@Fe_3O_4@Au nanoparticles. In these synthesis procedures, Fe_3O_4 and Au nanoparticles are assembled on amino-modified silica templates successively through electrostatic interactions. As shown in Figure 1b, tens of Fe_3O_4 nanoparticles can be found on the surfaces of a single SiO_2 nanoparticle. The TEM image of the SiO_2@Au@Fe_3O_4@PANI hybrids was shown in Figure 1d, where the PANI polymer coating can be clearly seen.

After the removal of SiO_2 templates, Au@Fe_3O_4@PANI hybrid shells with good monodispersibility were obtained (Figure 2a,b). Figure 2c displays the typical TEM image of a single Au@Fe_3O_4@PANI nanoparticle. It was interesting to find that Au nanoparticles tended to attach to the already existing Fe_3O_4 seeds on the SiO_2 templates to form a unique Fe_3O_4–Au Janus structure, which gave the possibility of interfacial communication between Au and Fe_3O_4. The typical HRTEM image of a single Fe_3O_4–Au Janus nanoparticle in the PANI shell is shown in Figure 2d. The interfringe distance was measured to be 0.24 nm for Au and 0.25 nm for Fe_3O_4, corresponding to the (111) plane of face-centered cubic (fcc)-structured Au and the (311) plane of inverse spinel-structured magnetite, respectively. The high-angle annular dark-field

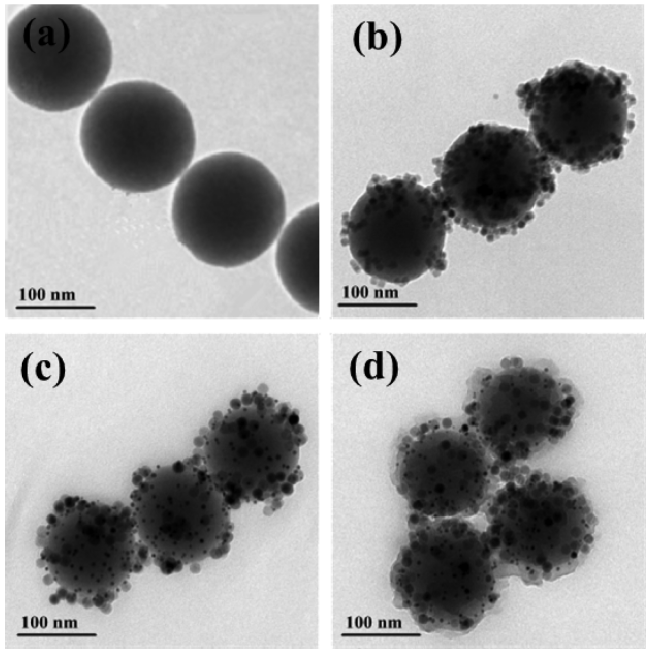

Figure 1. TEM images of (a) SiO_2, (b) SiO_2@Fe_3O_4, (c) SiO_2@Fe_3O_4@Au, and (d) SiO_2@Fe_3O_4@Au@PANI.

scanning transmission electron microscopy (HAADF-STEM) image was recorded to confirm the structure of Au@Fe_3O_4@PANI hybrid shells. As shown in Figure 2e, the Au and Fe_3O_4 nanoparticles show different brightness as the brightness is proportional to the atomic number (Z).[20,21] Under this circumstance, the Au nanoparticles appear brighter than Fe_3O_4 nanoparticles because of their higher Z. The energy-dispersive X-ray spectroscopic (EDS) elemental maps (Figure 2f–i) further confirm the expected Au@Fe_3O_4@PANI hybrid shell structure.

The concentration of aniline monomer was found to affect the integrity and thickness of the PANI shell. For clarity, the products were denoted as Au@Fe_3O_4@PANI(x), where x is the added amount of aniline monomer (in μL). As for the Au@Fe_3O_4@PANI(6) hybrid shell, the PANI shells are approximately 10 nm in thickness, which is too thin to cover all Fe_3O_4 nanoparticles (Figure 2c). The PANI shells become complete with most Fe_3O_4 and Au nanoparticles buried inside when the thickness of PANI shells is increased to 20 nm (Au@Fe_3O_4@PANI(9) hybrid shells, Figure 3a,c). The thickness of PANI shells can be further increased to 35 nm for Au@Fe_3O_4@PANI(12) hybrid shells (Figure 3b,d).

Figure 4a shows the FTIR spectra of SiO_2@Fe_3O_4@Au core–shell nanoparticles and Au@Fe_3O_4@PANI hybrid shells. In comparison with SiO_2@Fe_3O_4@Au core–shell nanoparticles, the characteristic absorption bands for PANI polymer in Au@Fe_3O_4@PANI hybrid shells can be indexed. The peaks at 1602 and 1500 cm^{-1} can be assigned to the quinonoid ring and the benzenoid ring, respectively,[22,23] and the peaks at 1172

DOI: 10.1021/acs.langmuir.7b00640
Langmuir 2017, 33, 4520–4527

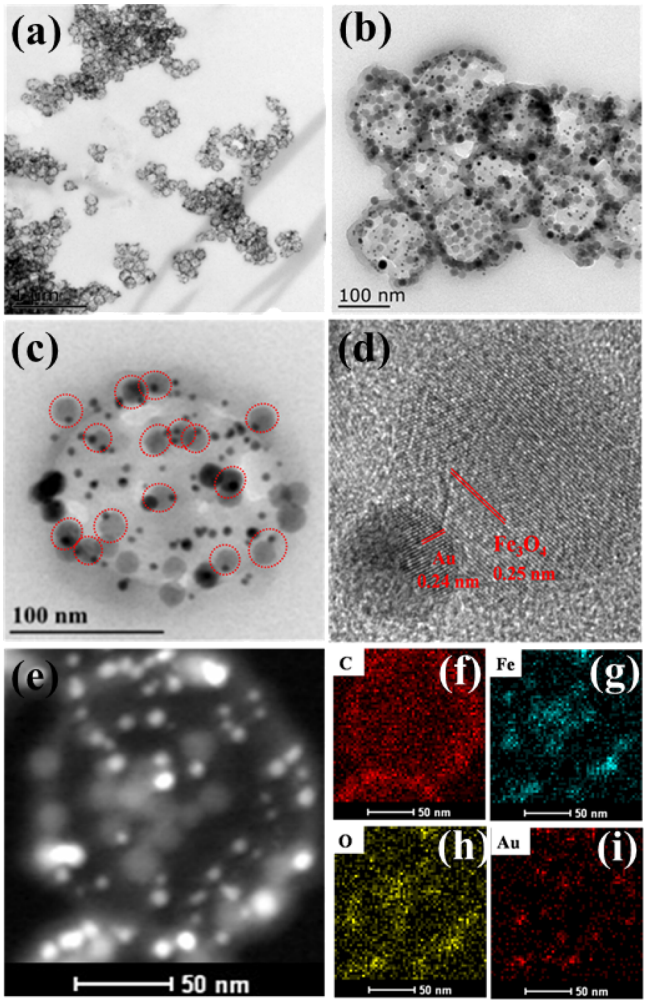

Figure 2. (a–c) TEM images of Au@Fe_3O_4@PANI(6) hybrid shells. (d) HRTEM image of a single Fe_3O_4–Au Janus nanoparticle in the PANI shell. (e) HAADF-STEM image of a single Au@Fe_3O_4@PANI(6) hybrid shell. (f–i) EDS maps of a single Au@Fe_3O_4@PANI(6) hybrid shell for (f) C, (g) Fe, (h) O, and (i) Au.

and 787 cm^{-1} can be assigned to the aromatic C–H in-plane bending modes and out-of-plane deformations of C–H bonds on 1,4-disubstituted rings,[24−26] respectively. XRD measurements were used to characterize the crystalline and phase structure of Au@Fe_3O_4@PANI hybrids. As observed in Figure 4b, the peaks at 38.18°, 44.40°, 64.68°, and 77.77° can be indexed to the (111), (200), (220) and (311) planes of fcc Au (JCPDS 04-0784), respectively, indicating the attachment of Au nanoparticles to silica templates. After the introduction of PANI, the SiO_2@Au@PANI core–shell nanoparticles show a broad band between 20° and 30°, which corresponded to amorphous PANI.[27] After the addition of Fe_3O_4 and the removal of SiO_2 templates, the broad band of PANI becomes clearer and the peaks at 2θ = 30.18°, 35.54°, 43.10°, 57.16°, and 62.78° can be ascribed to the (220), (311), (400), (511), and (440) planes of fcc Fe_3O_4 (JCPDS 19-0629), respectively. Figure 4c shows the UV–vis spectra of SiO_2@Au, SiO_2@Fe_3O_4@Au, and Au@Fe_3O_4@PANI hybrids. SiO_2@Au nanoparticles display a surface plasmon resonance peak of Au at 540 nm. After the addition of Fe_3O_4, the surface plasmon resonance peak shows a 13 nm blue shift to 527 nm. The change in the surface plasmon resonance confirms the interface communication between Au and Fe_3O_4, which will contribute to the improvement in the catalytic activity. When PANI was further introduced, the surface plasmon resonance peak of Au was covered by the strong adsorption of PANI. The chemical compositions and chemical states were then detected using XPS. As presented in Figure 4d, the Au 4f doublet peaks of SiO_2@Au particles can be located at the binding energies of 83.6 and 87.3 eV with the splitting of the 4f doublet of 3.7 eV, indicating that Au exists only in its metallic state. The Au 4f doublet peaks of SiO_2@Au@Fe_3O_4 core–shell nanoparticles shifted to 83.9 and 87.6 eV, and the peaks of Au@Fe_3O_4@PANI hybrid shells further shifted to 84.1 and 87.8 eV, indicating the existence of not only the interface communication between Au and Fe_3O_4 but also the communication between Au and PANI. The VSM was used to investigate the magnetic properties of the as-prepared Au@Fe_3O_4@PANI hybrids. As shown in Figure 4e, no remanence or coercivity was detected at room temperature, indicating their superparamagnetic character. The saturation magnetization of Au@Fe_3O_4@PANI hybrids is 65.46 emu/g, which means the easy separation of the as-prepared Au@Fe_3O_4@PANI hybrid shells from reaction mixtures with a low magnetic field gradient (insets in Figure 4e). N_2 adsorption–desorption measurements were used to reveal the surface properties (Figure 4f). The surface area of the Au@Fe_3O_4@PANI hybrid shells is 61.08 m^2 g^{-1}, and the average pore diameter calculated from the desorption curve is 4 nm (inset in Figure 4f).

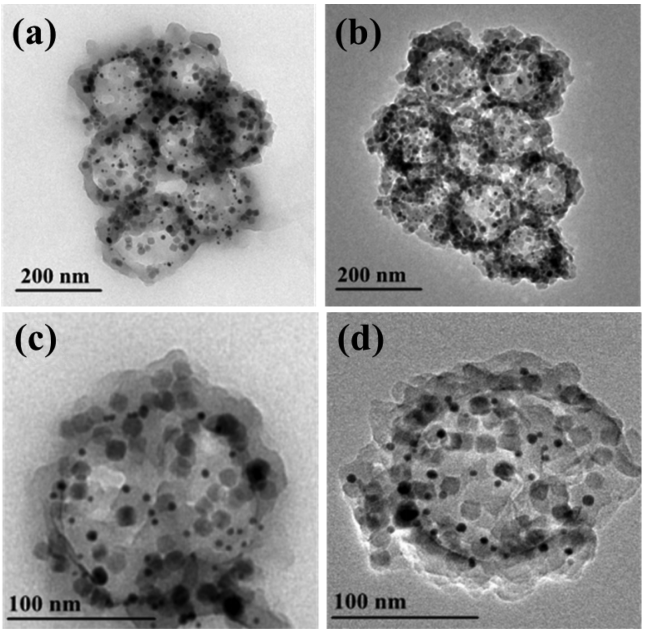

Figure 3. TEM images of (a,c) Au@Fe_3O_4@PANI(9) and (b,d) Au@Fe_3O_4@PANI(12).

2.2. Catalytic Performances of Au@Fe_3O_4@PANI Hybrid Shells. A model reaction, the reduction of 4-NP to 4-AP in the presence of $NaBH_4$, was chosen to monitor the catalytic performance of the as-formed Au@Fe_3O_4@PANI hybrid shells. The mixtures of 4-NP and $NaBH_4$ show an adsorption band at 400 nm corresponding to the 4-NP ions under alkaline conditions. After the addition of catalysts to the above reaction mixture, the peak at 400 nm successively decreases and another peak at 300 nm appears because of the formation of 4-AP (Figure 5a–c). It is commonly accepted that when Au nanoparticles are used for catalytic reduction, BH_4^-

DOI: 10.1021/acs.langmuir.7b00640
Langmuir 2017, 33, 4520–4527

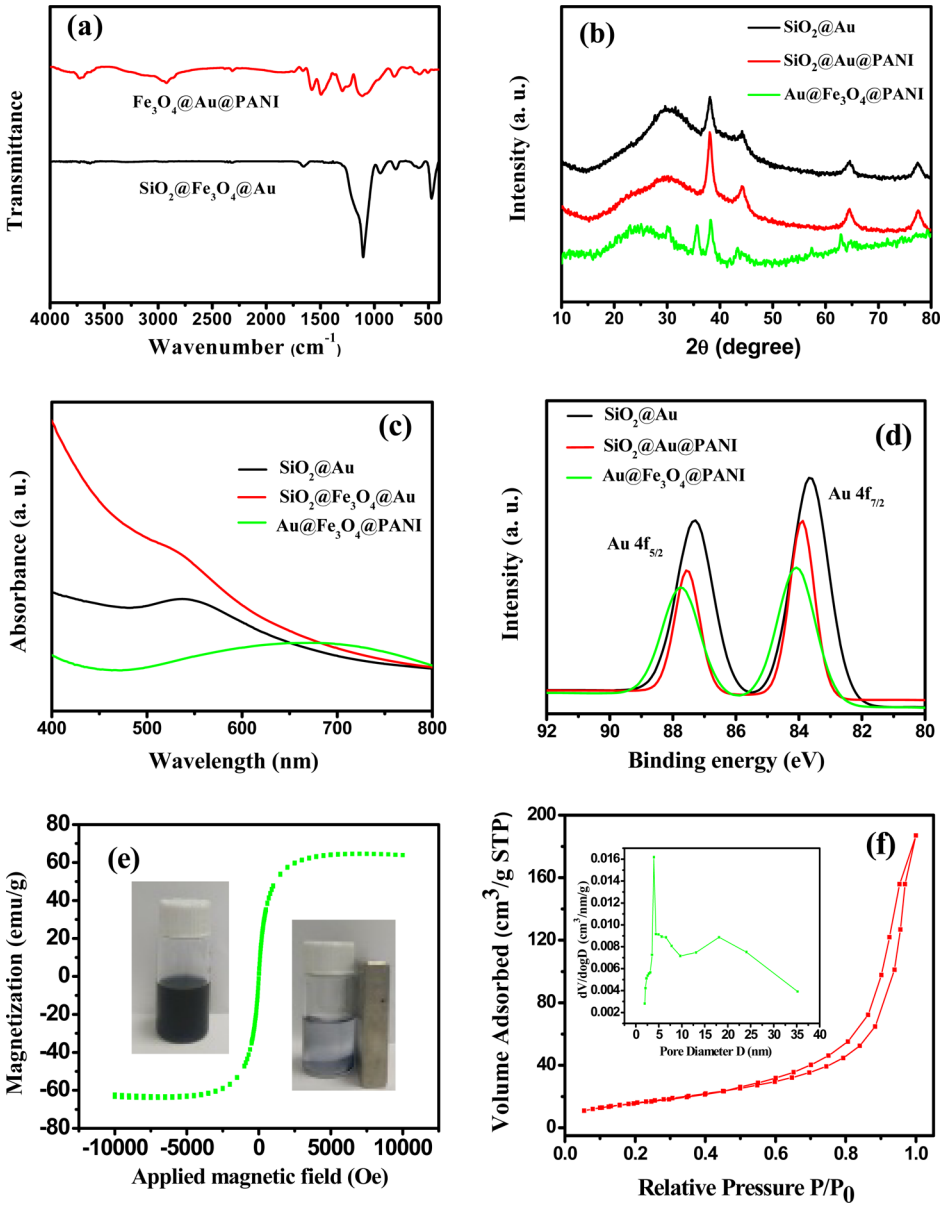

Figure 4. (a) FTIR of SiO_2@Fe_3O_4@Au and Au@Fe_3O_4@PANI. (b) XRD patterns of SiO_2@Au, SiO_2@Au@PANI, and Au@Fe_3O_4@PANI. (c) UV−vis spectra of SiO_2@Au, SiO_2@Fe_3O_4@Au, and Au@Fe_3O_4@PANI. (d) XPS spectra of Au 4f of SiO_2@Au, SiO_2@Au@PANI, and Au@Fe_3O_4@PANI. (e) Hysteresis loops of Au@Fe_3O_4@PANI hybrid shells; insets show the photographs of aqueous colloidal solution of Au@Fe_3O_4@PANI hybrid shells (left) before and (right) after the introduction of a magnet. (f) N_2 adsorption−desorption isotherms and corresponding pore size distribution of Au@Fe_3O_4@PANI hybrid shells.

and 4-NP are first diffused from the aqueous solution to the Au surfaces, and then, Au nanoparticles serve as catalysts to transfer electrons from BH_4^- to 4-NP, leading to the formation of 4-AP.[28,29]

Figure 5a−c shows the time-dependent adsorption spectra of the reaction solution in the presence of SiO_2@Au, SiO_2@Fe_3O_4@Au, and Au@Fe_3O_4@PANI hybrids as catalysts. The peak at 400 nm successively decreases, and another peak at 300 nm appears because of the formation of 4-AP. It is worth noting that the adsorption effect of PANI toward 4-NP should be taken into consideration. As shown in Figure 5a−c, the adsorption equilibrium can be reached within 2 min. The reduction of 4-NP to 4-AP was totally finished within 10, 7, and 5 min (after deducting the absorption time) using SiO_2@Au, SiO_2@Fe_3O_4@Au, and Au@Fe_3O_4@PANI(9) hybrids as catalysts, respectively. Because the reduction of 4-NP by $NaBH_4$ does not occur without catalysts and the $NaBH_4$ concentration in the reaction is much more excess, the reaction can be considered to fit the first-order rate law with respect to the concentration of 4-NP.[30] The linear relation of $\ln(C_t/C_0)$ versus time was observed for different catalysts (Figure 5d), where the concentration of 4-NP at time t and time 0 was recorded as C_t and C_0, respectively. The rate constant (k) of SiO_2@Au, SiO_2@Fe_3O_4@Au, and Au@Fe_3O_4@PANI(9) as catalysts was estimated to be 0.261, 0.353, and 0.433 min^{-1}, respectively. In addition, the turnover frequency (TOF) also follows the same sequence. The results indicate that both Fe_3O_4 and PANI contribute to the enhanced catalytic activity of Au (Figure 5e). The catalytic activity of Au@Fe_3O_4@PANI hybrid shells is superior to those of the reported PANI- and/or Fe_3O_4-supported noble metal nanocatalysts (Table S1). It is believed that the improvement in the catalytic activity of Au@Fe_3O_4@

DOI: 10.1021/acs.langmuir.7b00640
Langmuir 2017, 33, 4520−4527

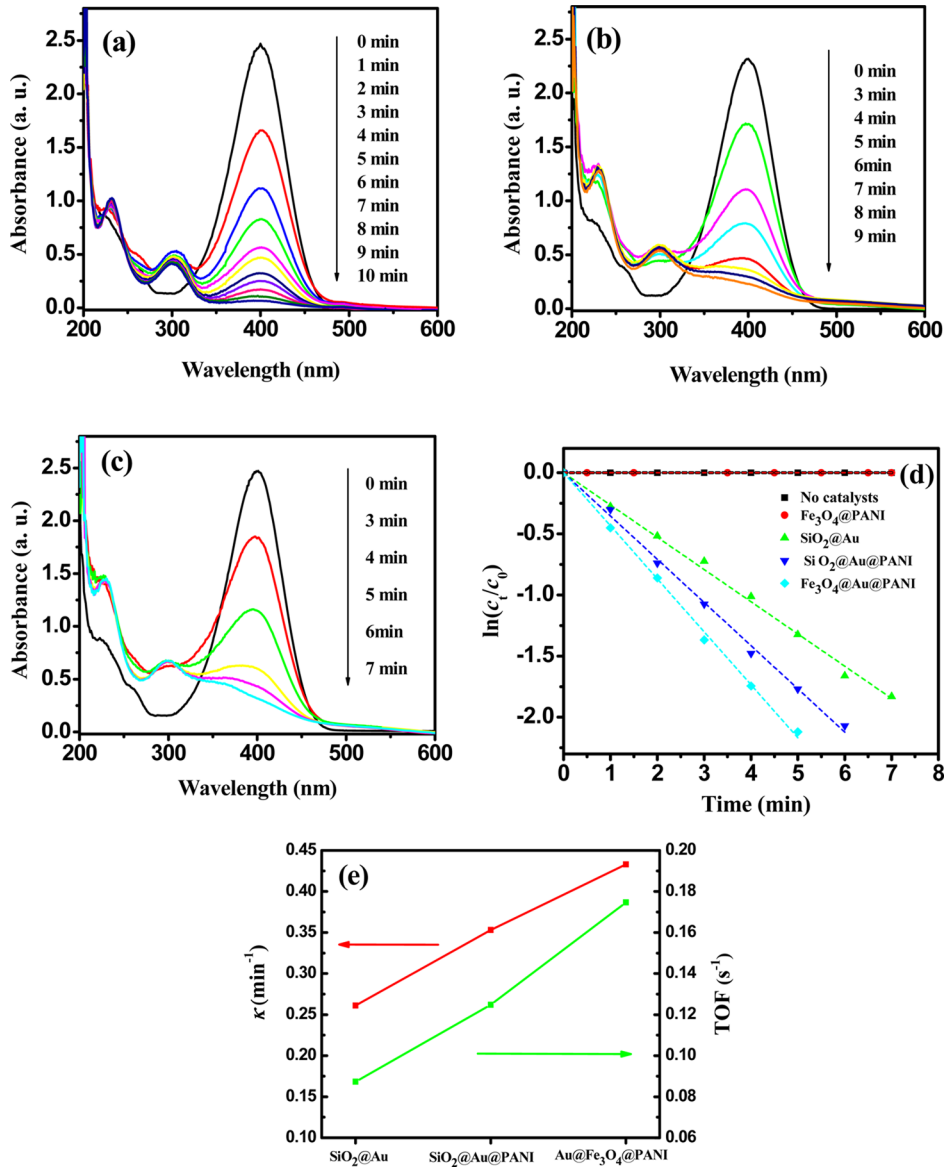

Figure 5. UV−vis spectra showing gradual reduction of 4-NP using (a) SiO_2@Au, (b) SiO_2@Au@PANI, and (c) Au@Fe_3O_4@PANI(9) in the first run. (d) Plots of $\ln(C_t/C_0)$ of 4-NP against time using different catalysts and (e) k and TOF of different catalysts.

PANI is due to the synergetic effect caused by electron transfer across the interface between both Au−PANI and Au−Fe_3O_4, which was confirmed using UV−vis and XPS analyses.

The catalytic activity of Au@Fe_3O_4@PANI hybrid shells with different thicknesses of PANI shells was also investigated. As shown in Figures 6a, 5c, and 6b, the reaction time first increases and then decreases as the thickness of the PANI shell increases, and the rate constant also follows the same sequence (Figure 6c). It is believed that when the PANI shell is too thin to cover all Au nanoparticles (Figure 2c), Au nanoparticles cannot make full contact with PANI. As a result, the synergetic effect between Au and PANI cannot be fully used. If the PANI shell is very thick (Figure 3d), it will take more time for the reaction molecules to establish contact with Au nanoparticles, which decrease the catalytic activity.

Magnetic property of the catalysts plays a vital role in catalytic reactions because it makes the separation and reuse of catalysts easier. As the as-formed Au@Fe_3O_4@PANI hybrid shells show excellent magnetic properties, they can be collected easily after the catalytic reduction. When unsupported Au nanoparticles are used as catalysts, they cannot be effectively collected after the catalytic reduction (Figure 6d). When Au nanoparticles are attached to SiO_2 nanoparticles, complete loss in the catalytic activity after the fourth run can be found because of the aggregation of Au nanoparticles. After the introduction of the PANI shell, the catalysts can be recycled for six runs. As for the Au@Fe_3O_4@PANI hybrid shells, they can be simply recycled using a magnet and reused for at least nine successive cycles with a stable conversion efficiency of approximately 100%. Besides, the original nanostructures remained after nine cycles. These results indicate their high recyclability and stability.

3. CONCLUSIONS

In conclusion, Au@Fe_3O_4@PANI hybrid shells as advanced supported catalysts have been fabricated. The catalytic results indicated that the introduction of PANI and Fe_3O_4 could largely improve the catalytic activity because of the synergetic

DOI: 10.1021/acs.langmuir.7b00640
Langmuir 2017, 33, 4520−4527

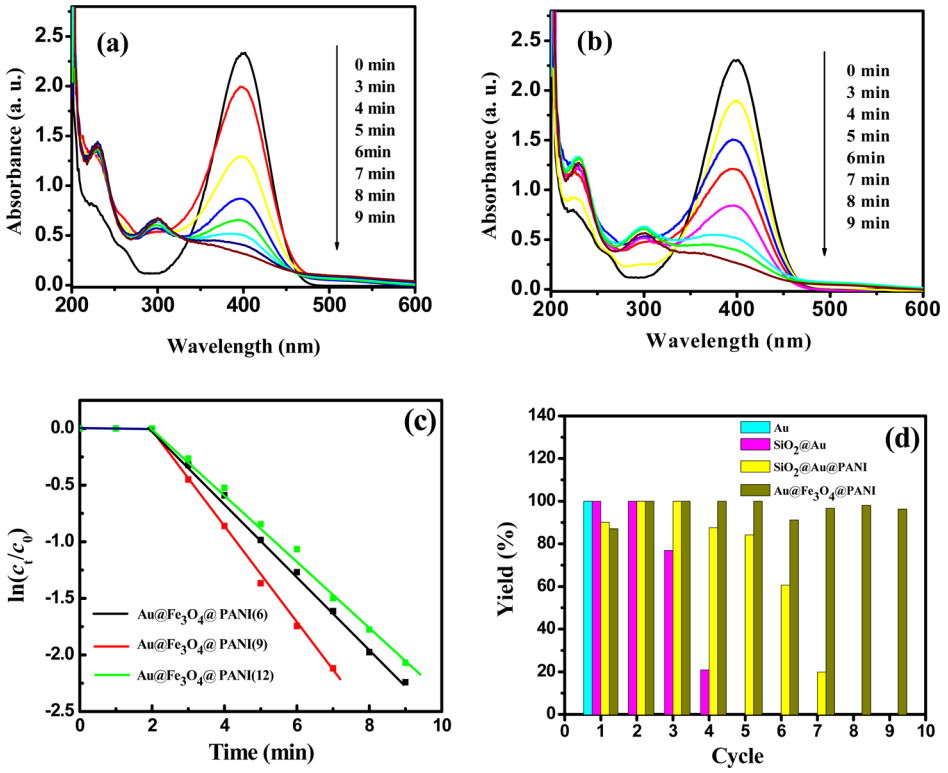

Figure 6. UV−vis spectra showing gradual reduction of 4-NP using (a) Au@Fe_3O_4@ PANI(6) and (b) Au@Fe_3O_4@ PANI(12) in the first run. (c) Plots of $\ln(C_t/C_0)$ of 4-NP against time using Au@Fe_3O_4@PANI hybrid shells with different PANI thicknesses and (d) synthesis yield of 4-AP in the successive reactions with different catalysts.

effects between both Au−PANI and Au−Fe_3O_4. In addition, PANI and Fe_3O_4 could also improve the stability and recyclability of Au nanoparticles by preventing them from aggregation. The superior catalytic performance of Au@Fe_3O_4@PANI hybrid shells clearly indicates their potential applications as efficient heterogeneous catalysts in liquid-phase catalysis. It should be noted that there are still Au nanoparticles not well-attached to Fe_3O_4 nanoparticles in this case, and further improvement in the catalytic activity of Au@Fe_3O_4@PANI hybrid shells is still possible by maximizing the synergetic effect between Au and Fe_3O_4, which will be our continuing interest.

4. EXPERIMENTAL METHODS

4.1. Materials. 1-Octadecene (ODE, 90%), *n*-tetracosane (TCA), 3,4-dihydroxyhydrocinnamic acid (DHCA), tetraethyl orthosilicate (TEOS), and (3-aminopropyl)triethoxysilane (APTES) were purchased from Sigma-Aldrich. Oleic acid, auric acid, and all other reagents were purchased from Sinopharm Chemical Reagent Co. Ltd. (China). The water used in this study was deionized and purified through a Millipore system.

4.2. Synthesis of Hydrophobic Fe_3O_4 Nanoparticles. The hydrophobic Fe_3O_4 nanoparticles were synthesized according to the literature.[18] First, iron oleate was prepared. Iron chloride (10.8 g) and oleate sodium (36.5 g) were dissolved in a mixture solvent involving 60 mL of distilled water, 80 mL of ethanol, and 140 mL of hexane. After the reaction, the solution was stirred until the sodium oleate was dissolved completely; the mixed reaction solution was heated to 60 °C and kept refluxing for 4 h. When the reaction was finished, the upper organic layer was washed three times with 90 mL of distilled water. After the removal of hexane using a rotary evaporator, the final product is a reddish-brown viscous oil. After that, 1.8 g of iron oleate and 0.285 g of oleic acid were dissolved in 10 g of ODE at room temperature under an N_2 atmosphere. After 20 min, the reaction solution was heated to 320 °C (~18 °C/min) and then kept at this temperature for 60 min. After, the resultant reaction solution containing the nanoparticles cooled to room temperature. The nanoparticles were washed three times with a mixture of hexane and acetone . The magnetic nanoparticles were dispersed into 36 mL of tetrahydrofuran (THF).

4.3. Ligand Exchange of Hydrophobic Fe_3O_4 Nanoparticles with DHCA. The hydrophobic magnetic nanoparticles were transferred into aqueous solution according to the literature with a reasonable modification.[19] DHCA (50 mg) was dissolved in 6 mL of THF followed by heating the resultant solution to 50 °C. Then, 6 mL of hydrophobic magnetic nanoparticles in THF were added dropwise. After stirring at this temperature for 3 h, the reaction solution was cooled to room temperature. To precipitate the Fe_3O_4 nanoparticles, 500 μL of NaOH (0.5 M) was then added to the solution. The precipitate was collected by centrifugation (4000 rpm) and redispersed into water for further use (1 mg/mL, pH = 4).

4.4. Synthesis of Au Nanoparticles. In a typical synthesis, 555.5 mg of polyvinylpyrrolidone (PVP-K30) was added to the $HAuCl_4$ aqueous solution (1 mM, 50 mL). The mixture was further stirred for 30 min in an ice bath. Then, $NaBH_4$ aqueous solution (0.1 M, 5 mL) was added into the mixture rapidly under vigorous stirring and kept under stirring for 10 min.

4.5. Synthesis of Surface-Modified SiO_2 Nanoparticles. Typically, ethanol (92 mL) was mixed with water (17.2 mL), ammonium aqueous solution (4 mL), and TEOS (3.44 mL). After stirring for 4 h at room temperature, the solids were separated by centrifugation and washed three times with water and ethanol . Then, the solids were dispersed into 30 mL of isopropanol and 0.4 mL of APTES. The mixture solution was refluxed for 3 h and then cooled to room temperature. The solid material was obtained by centrifugation and redispersed into water for further use (1 mg/mL, pH = 4).

4.6. Synthesis of SiO_2@Au@Fe_3O_4 Core−Shell Nanoparticles. In a typical synthesis, 12 mL of as-formed NH_2−SiO_2 aqueous solution was mixed with 4 mL of DHCA−Fe_3O_4 aqueous solution and stirred for 4 h at room temperature. After that, the precipitate was

DOI: 10.1021/acs.langmuir.7b00640
Langmuir 2017, 33, 4520−4527

collected by centrifugation, redispersed into 12 mL of water (pH = 4), and mixed with 4 mL of as-prepared Au aqueous solution. After stirring at room temperature for 4 h, the solid material was obtained by centrifugation.

4.7. Synthesis of Au@Fe_3O_4@PANI Hybrid Shells. The as-formed SiO_2@Au@Fe_3O_4 hybrid shells were dispersed into 5 mL of deionized water. Subsequently, a certain amount of aniline was added to the above solution (pH = 1), and the solution was stirred in an ice bath for 2 h. Then, ammonium persulfate (APS) dissolved in 1 mL of deionized water (molar ratio of APS to aniline was set at 1:1) was added into the reaction solution, and the solution was stirred for 4 h. After that, the precipitate was collected by centrifugation and washed three times with deionized water and ethanol. The as-prepared SiO_2@Au@Fe_3O_4@PANI core−shell nanoparticles were dispersed into 5 mL of water, followed by adding 0.4 g of NaOH and stirring at 70 °C for 4 h. After the solution was cooled to room temperature, the Au@Fe_3O_4@PANI hybrid shells were obtained by centrifugation, washed three times with water and ethanol , and then dispersed into 4 mL of water for further use.

4.8. Catalytic Reaction. Typically, an aqueous solution of $NaBH_4$ (1.0 mL, 1.5×10^{-2} M) and 4-NP (1.7 mL, 2.0×10^{-4} M) was added into a quartz cell (1 cm path length), followed by adding 25 μL of as-prepared catalysts. Then, the progress of the conversion of 4-NP to 4-aminophenol (4-AP) was monitored using the UV−vis spectroscopy, which could record the time-dependent adsorption spectra of the reaction mixture with a time interval of certain minutes in a scanning range of 200−600 nm at ambient temperature. After each run, the catalysts were collected using a magnet, purified twice with water, and then redispersed into water for further use in the next cycle.

4.9. Characterization. Morphologies were characterized using transmission electron microscopy (TEM, JEM-2100 F) and high-resolution TEM (HRTEM, Tecnai G2 F30 S-Twin TEM, FEI) instruments. The crystal phase was analyzed using X-ray diffraction (XRD) using a Bruker AXS D8 ADVANCE X-ray diffractometer. The products were recorded in the 2θ range from 10° to 80.0° in steps of 0.04° with a count time of 1 s each time. Fourier transform infrared (FTIR) spectra of the products were recorded in the range of 400−4000 cm^{-1} using FTIR spectroscopy (Tensor 27, Bruker, Germany). The samples were prepared in a pellet form with spectroscopic-grade KBr. UV−vis diffuse reflectance spectra (Cary 5000, Varian) was used to test the optical properties. The Axis Ultra X-ray photoelectron spectroscope (XPS, Kratos Analytical Ltd., UK) equipped with a standard monochromatic Al Kα source ($h\nu$ = 1486.6 eV) was used to measure the phase composition. The binding energy of the photoelectrons was determined under the assumption that Au has a binding energy of 84.0 eV. Magnetic measurements were recorded using a vibrating sample magnetometer (VSM, EV7, ADE, USA) with a maximum applied continuous field of 10 000 Oe at room temperature. The specific surface and the pore size were measured using a Beishide 3H-2000PS2 analysis instrument. The surface area was determined from the adsorption isotherm using the multipoint Brunauer−Emmett−Teller method in the pressure P/P_0 range of 0.04−0.32. The desorption isotherm was used to determine the average pore size and distribution using the Barrett−Joyner−Halenda method.

■ ASSOCIATED CONTENT

Supporting Information

The Supporting Information is available free of charge on the ACS Publications website at DOI: 10.1021/acs.langmuir.7b00640.

Comparison of catalytic activity of different catalysts (Table S1) (PDF)

■ AUTHOR INFORMATION

Corresponding Authors

*E-mail: hanjie@yzu.edu.cn (J.H.).
*E-mail: guorong@yzu.edu.cn (R.G.).

ORCID

Jie Han: 0000-0003-0050-7509
Rong Guo: 0000-0001-7554-3948

Notes

The authors declare no competing financial interest.

■ ACKNOWLEDGMENTS

The authors gratefully acknowledge financial support from the National Natural Science Foundation of China (21673202 and 21273004), Qing Lan Project, and the Priority Academic Program Development of Jiangsu Higher Education Institutions. We would also like to acknowledge the technical support received at the Testing Center of Yangzhou University.

■ REFERENCES

(1) Haruta, M.; Kobayashi, T.; Sano, H.; Yamada, N. Novel Gold Catalysts for the Oxidation of Carbon Monoxide at a Temperature Far Below 0 °C. *Chem. Lett.* **1987**, *16*, 405−408.

(2) Shih, H.-H.; Williams, D.; Mack, N. H.; Wang, H.-L. Conducting polymer-based electrodeless deposition of Pt nanoparticles and its catalytic properties for regioselective hydrosilylation reactions. *Macromolecules* **2009**, *42*, 14−16.

(3) Liu, Y.; Goebl, J.; Yin, Y. Templated synthesis of nanostructured materials. *Chem. Soc. Rev.* **2013**, *42*, 2610−2653.

(4) Han, J.; Wang, M.; Chen, R.; Han, N.; Guo, R. Beyond yolk−shell nanostructure: A single Au nanoparticle encapsulated in the porous shell of polymer hollow spheres with remarkably improved catalytic efficiency and recyclability. *Chem. Commun.* **2014**, *50*, 8295−8298.

(5) Lin, F.-h.; Doong, R.-a. Bifunctional Au−Fe_3O_4 heterostructures for magnetically recyclable catalysis of nitrophenol reduction. *J. Phys. Chem. C* **2011**, *115*, 6591−6598.

(6) Han, J.; Lu, S.; Jin, C.; Wang, M.; Guo, R. Fe_3O_4/PANI/m-SiO_2 as robust reactive catalyst supports for noble metal nanoparticles with improved stability and recyclability. *J. Mater. Chem. A* **2014**, *2*, 13016−13023.

(7) Li, Y.; Zhang, Z.; Fan, T.; Li, X.; Ji, J.; Dong, P.; Baines, R.; Shen, J.; Ye, M. Magnetic core−shell to yolk−shell structures in palladium-catalyzed Suzuki−Miyaura reactions: Heterogeneous versus homogeneous nature. *ChemPlusChem* **2016**, *81*, 564−573.

(8) Ge, J.; Zhang, Q.; Zhang, T.; Yin, Y. Core-satellite nanocomposite catalysts protected by a porous silica shell: Controllable reactivity, high stability, and magnetic recyclability. *Angew. Chem., Int. Ed.* **2008**, *47*, 8924−8928.

(9) Wang, C.; Daimon, H.; Sun, S. Dumbbell-Like Pt−Fe_3O_4 Nanoparticles and Their Enhanced Catalysis for Oxygen Reduction Reaction. *Nano Lett.* **2009**, *9*, 1493−1496.

(10) Sheng, Y.; Xue, J. Synthesis and properties of Au−Fe_3O_4 heterostructured nanoparticles. *J. Colloid Interface Sci.* **2012**, *374*, 96−101.

(11) Wei, Y.; Klajn, R.; Pinchuk, A. O.; Grzybowski, B. A. Synthesis, shape control, and optical properties of hybrid Au/Fe_3O_4 "nanoflowers". *Small* **2008**, *4*, 1635−1639.

(12) Jin, C.; Qu, Y.; Wang, M.; Han, J.; Hu, Y.; Guo, R. Aqueous solution-based Fe_3O_4 seed-mediated route to hydrophilic Fe_3O_4−Au Janus nanoparticles. *Langmuir* **2016**, *32*, 4595−4601.

(13) Luo, J.; Zhong, W.; Zou, Y.; Xiong, C.; Yang, W. Preparation of morphology-controllable polyaniline and polyaniline/graphene hydrogels for high performance binder-free supercapacitor electrodes. *J. Power Sources* **2016**, *319*, 73−81.

(14) Yang, C.; Chen, Z.; Shakir, I.; Xu, Y.; Lu, H. Rational synthesis of carbon shell coated polyaniline/MoS_2 monolayer composites for high-performance supercapacitors. *Nano Res.* **2016**, *9*, 951−962.

(15) Xue, X.; Fu, Y.; Wang, Q.; Xing, L.; Zhang, Y. Outputting olfactory bionic electric impulse by PANI/PTFE/PANI sandwich nanostructures and their application as flexible, smelling electronic skin. *Adv. Funct. Mater.* **2016**, *26*, 3128−3138.

DOI: 10.1021/acs.langmuir.7b00640
Langmuir 2017, 33, 4520−4527

(16) Han, J.; Wang, M.; Cao, S.; Fang, P.; Lu, S.; Chen, R.; Guo, R. Reactive template strategy for fabrication of MnO_2/polyaniline coaxial nanocables and their catalytic application in the oxidative decolorization of rhodamine B. *J. Mater. Chem. A* **2013**, *1*, 13197−13202.
(17) Liu, Y.; Chen, T.; Wu, C.; Qiu, L.; Hu, R.; Li, J.; Cansiz, S.; Zhang, L.; Cui, C.; Zhu, G.; You, M.; Zhang, T.; Tan, W. Facile surface functionalization of hydrophobic magnetic nanoparticles. *J. Am. Chem. Soc.* **2014**, *136*, 12552−12555.
(18) Stöber, W.; Fink, A.; Bohn, E. Controlled growth of monodisperse silica spheres in the micron size range. *J. Colloid Interface Sci.* **1968**, *26*, 62−69.
(19) Park, J.; An, K.; Hwang, Y.; Park, J.-G.; Noh, H.-J.; Kim, J.-Y.; Park, J.-H.; Hwang, N.-M.; Hyeon, T. Ultra-large-scale syntheses of monodisperse nanocrystals. *Nat. Mater.* **2004**, *3*, 891−895.
(20) Yu, H.; Chen, M.; Rice, P. M.; Wang, S. X.; White, R. L.; Sun, S. Dumbbell-like bifunctional Au−Fe_3O_4 nanoparticles. *Nano Lett.* **2005**, *5*, 379−382.
(21) Nellist, P. D.; Pennycook, S. J. Incoherent imaging using dynamically scattered coherent electrons. *Ultramicroscopy* **1999**, *78*, 111−124.
(22) Liu, W.; Kumar, J.; Tripathy, S.; Senecal, K. J.; Samuelson, L. Enzymatically synthesized conducting polyaniline. *J. Am. Chem. Soc.* **1999**, *121*, 71−78.
(23) Kang, E. T.; Neoh, K. G.; Tan, K. L. Polyaniline: A polymer with many interesting intrinsic redox states. *Prog. Polym. Sci.* **1998**, *23*, 277−324.
(24) Zhang, G.; Xia, B. Y.; Wang, X.; Lou, X. W. D. Strongly coupled $NiCo_2O_4$-rGO hybrid nanosheets as a methanol-tolerant electrocatalyst for the oxygen reduction reaction. *Adv. Mater.* **2014**, *26*, 2408−2412.
(25) Feng, Y.; Alonso-Vante, N. Nonprecious metal catalysts for the molecular oxygen-reduction reaction. *Phys. Status Solidi B* **2008**, *245*, 1792−1806.
(26) Chen, Z.; Higgins, D.; Yu, A.; Zhang, L.; Zhang, J. A review on non-precious metal electrocatalysts for PEM fuel cells. *Energy Environ. Sci.* **2011**, *4*, 3167−3192.
(27) Han, J.; Li, L.; Guo, R. Novel approach to controllable synthesis of gold nanoparticles supported on polyaniline nanofibers. *Macromolecules* **2010**, *43*, 10636−10644.
(28) Pradhan, N.; Pal, A.; Pal, T. Silver nanoparticle catalyzed reduction of aromatic nitro compounds. *Colloids Surf., A* **2002**, *196*, 247−257.
(29) Huang, J.; Vongehr, S.; Tang, S.; Lu, H.; Shen, J.; Meng, X. Ag dendrite-based Au/Ag bimetallic nanostructures with strongly enhanced catalytic activity. *Langmuir* **2009**, *25*, 11890−11896.
(30) Panigrahi, S.; Basu, S.; Praharaj, S.; Pande, S.; Jana, S.; Pal, A.; Ghosh, S. K.; Pal, T. Synthesis and size-selective catalysis by supported gold nanoparticles: Study on heterogeneous and homogeneous catalytic process. *J. Phys. Chem. C* **2007**, *111*, 4596−4605.

DOI: 10.1021/acs.langmuir.7b00640
Langmuir 2017, 33, 4520−4527